Effect of TiC Particle Additions on Structure and Properties of Hypereutectic High Chromium Cast Iron

Han-guang Fu, Xiao-jun Wu, Xue-yi Li, Jian-dong Xing, Yong-ping Lei, and Xiao-hui Zhi

The present work studies the effects of titanium carbide (TiC) particle additions on the microstructure and mechanical properties of hypereutectic high chromium cast iron containing about 20%Cr and 4.0%C by the optical microscopy (OM), the transmission electron microscopy (TEM), the X-ray diffraction (XRD) analysis, the digital image analysis system, impact tester, and hardness tester. The carbides of high chromium cast iron are refined gradually and the shape of the primary M_7C_3-type carbides became more isotropic with the increase of TiC particles. When the addition of TiC particles exceeds 1.0 wt.%, the change of microstructure is not obvious. The hardness of high chromium cast iron has a slight increase and impact toughness has a obvious increase with the increase of TiC additions. However, when the addition of TiC particles exceeds 1.0 wt.%, the impact toughness has no obvious change.

1. Introduction

Superior abrasive wear resistance, combined with relatively low production costs, makes high Cr white cast irons (WCIs) particularly attractive for applications in the grinding, milling, and pumping apparatus used to process hard materials (Ref 1-4). The wear resistance of high Cr WCIs is due to their microstructure, which comprises hard rod-like carbides dispersed in a matrix of austenite or martensite. Many investigations had discovered that the increase of carbide volume fraction could increase the abrasive wear resistance of high Cr WCIs (Ref 5, 6). However, the hypereutectic high chromium cast irons (HHCCIs) with over 3.6% C generally are not favored for casting, due to high scrap and high rejection rate which are mainly caused by the coarser and larger primary carbides (Ref 7-9). The refinement of primary carbides can decrease the brittleness of HHCCIs and benefits to enlarge the application of HHCCIs.

Xing et al. (Ref 10-12) investigated the effect of titanium, niobium, and cerium elements on the morphology of primary M_7C_3 carbides in the HHCCIs and discovered that titanium, niobium, and cerium elements could refine the primary M_7C_3 carbides in the HHCCIs. Atamert and Bhadeshia (Ref 13, 14) found that the shape of the normally elongated and rather brittle

M_7C_3 carbides was altered to a more equiaxed morphology using silicon element. The additions of some alloy elements that segregate to the matrix/carbide interphase, such as magnesium, boron, potassium, etc., have also been used to modify the eutectic carbide structure and these attempts generally have improved the morphology and size of the eutectic carbides (Ref 15-18). Moreover, the additions of tungsten carbide (WC) particles in the solidification of low chromium WCIs can refine the as-cast structure of low chromium WCIs and increase its impact toughness by 28.0% and its abrasive wear resistance by 63.6% (Ref 19). The addition of 0.5 vol.% titanium carbide (TiC) particle can refine the microstructure of ZA84 magnesium alloy (Mg-8Zn-4Al-0.25Mn) and convert the ternary phase in the microstructure from the coarse quasi-continuous network into fine discontinuous network with more dispersive distribution. It can also improve the mechanical properties, creep resistance, and castability of the magnesium alloy (Ref 20).

The objectives of present research are to refine the larger primary carbides of the HHCCIs and increase the impact toughness of HHCCIs and enlarge its application in the slurry pump by the addition of titanium carbide (TiC) particles. In this paper, we investigate the effect of TiC particle additions on the microstructure and mechanical properties of HHCCIs, and discover that the addition of TiC particles can obviously refine the carbide and increase the impact toughness of HHCCIs. The effect of TiC particle additions on the abrasive wear resistance of HHCCIs will be the subject of a future paper.

2. Experimental

A master alloy cast iron used in the present work was prepared from high carbon ferro-chromium (62%Cr), the low carbon steel, and pig iron by using a 100 kg capacity medium frequency electric furnace. The melt was poured into a sand mold and allowed to cool. The chemical compositions (in wt.%) of master alloy cast iron were as follows: 4.03C, 19.99Cr, 0.33Si, 0.42Mn, 0.028S, 0.034P, and balance Fe. From this

Han-guang Fu and **Yong-ping Lei**, Research Institute of Advance Materials Processing Technology, School of Materials Science and Engineering, Beijing University of Technology, Beijing 100124, P.R. China; **Han-guang Fu, Xiao-jun Wu, Jian-dong Xing,** and **Xiao-hui Zhi**, School of Materials Science and Engineering, Xi'an Jiaotong University, Xi'an 710049 Shaanxi Province, P.R. China; and **Xue-yi Li**, School of Mechanical and Electronic Engineering, Shandong University of Science and Technology, Qingdao 266510 Shandong Province, P.R. China. Contact e-mail: fhg64@263.net.

master alloy cast iron, 10 kg samples of material were remelted in a 10 kg capacity furnace. The melt was subsequently superheated to 1560 °C and transferred into a pre-heated ladle, the preheating temperature of ladle was 350-400 °C. TiC particles with diameter of about 2.8 μm were deposited in the bottom of the ladle, and then the melt containing TiC particles was stirred with a steel bar. The additions of TiC particles were as follows: (a) 0% TiC (Sample A_0); (b) 0.5 wt.% TiC (Sample A_1); (c) 1.0 wt.% TiC (Sample A_2); and (d) 1.5 wt.% TiC (Sample A_3). Above alloys were then cast at 1380 °C into the sand molds to produce ingots of dimensions of $60 \times 60 \times 200$ mm.

The specimens were metallographically polished and etched with 5% nital. The microstructures at the location of 1.0 mm under the surface were characterized utilizing Neophot 32 optical microscope (OM) and JEM 3010 transmission electron microscope (TEM). X-ray diffraction (XRD) was carried out on an MXP21VAHF diffractometer with Copper Kα radiation at 40 kV and 200 mA as an X-ray source. The sample was scanned in the 2θ range of 20-85° in a step-scan mode (0.02° per step). The micrographs correspond to the transverse section of the columnar carbides. The average carbide diameters D at the position are used to determine the refining effect of TiC particles on the carbides, which is given by the following equation:

$$D = 2\sqrt{\frac{A}{N\pi}} \qquad \text{(Eq 1)}$$

where A is area of the carbides and N is the number of the carbides in one image.

With this arrangement, 20 images of each specimen at magnification of 200 times are randomly selected and processed for the calculation of D using the LEICA digital image analysis system on the deep-etched specimens. The measurement of volume fraction of carbides used a LEICA digital images analyzer on the deep-etched specimens also.

Moreover, impact toughness (a_k, J/cm^2, it is impact toughness of materials and defined as the sample absorbing impact energy divided by cross section area of the sample) was performed on a JB-36 type impact tester, the dimensions of specimens were $20 \times 20 \times 110$ mm, no notch. The impact load was 294 N. The toughness values were the average of three specimens. The hardness at room temperature was measured by HR-150D type hardmeter. The results plotted in this paper are the averages of three specimens. The microhardness of matrix in the HHCCIs was measured by using a Vickers microhardness tester and a load of 0.5 N. At least seven indentations were made on each sample under each experimental condition to check reproducibility of the hardness data.

3. Experimental Results and Discussion

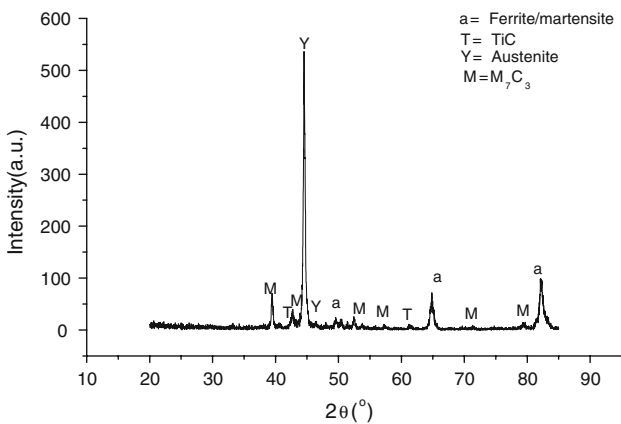### 3.1 Effect of TiC Additions on Microstructure of HHCCIs

Figure 1 shows the optical micrographs at the location of 1.0 mm below the surface. Figure 2 shows the change of average carbide diameters D with different TiC additions. From Fig. 1 and 2, it can be seen that carbides are refined gradually and the shape of the primary M_7C_3-type carbides became more isotropic
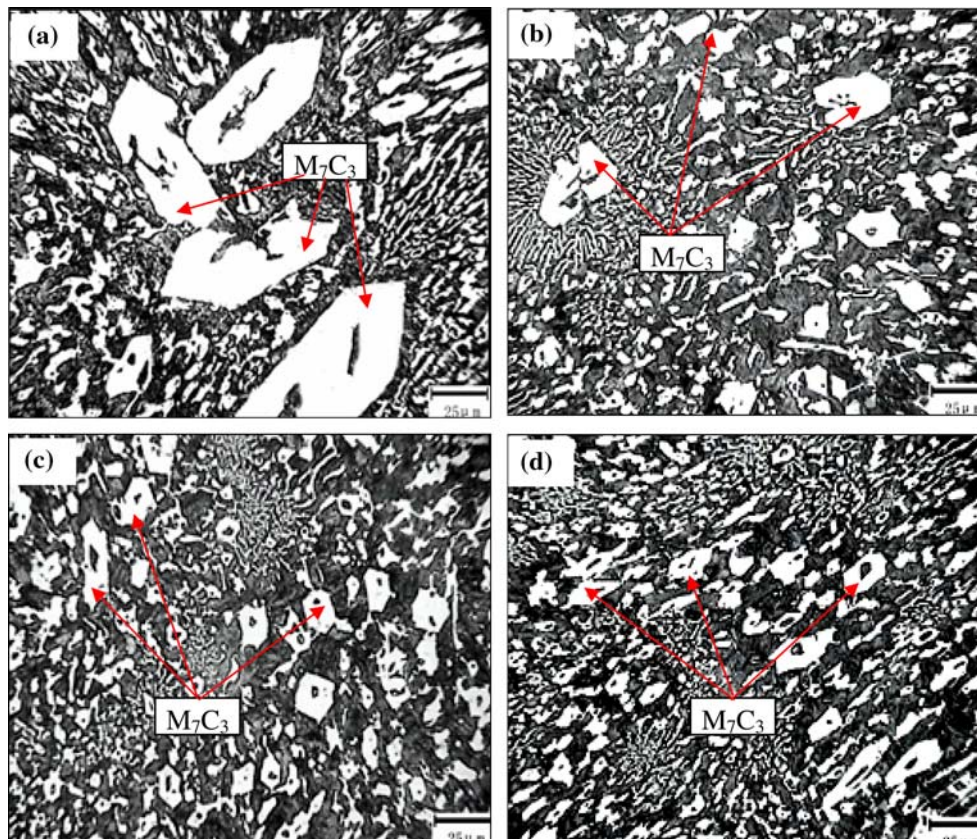
Fig. 1 Microstructures at 1.0 mm under the surface: (a) A_0 sample; (b) A_1 sample; (c) A_2 sample; (d) A_3 sample
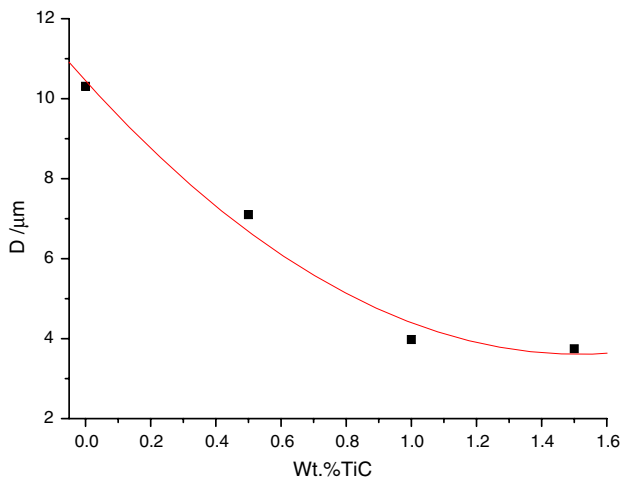
Fig. 2 Relationship between the equivalent diameter of carbides and TiC additions

Matching interface	$[uvw]_s$	$[uvw]_n$	d_s, nm	d_n, nm	θ, °C	δ, %
$(110)_{TiC}//(01\overline{1}0)_{M_7C_3}$	001	0001	0.432	0.454	0	8.4
	$\overline{1}10$	$\overline{1}2\overline{1}0$	0.611	0.688	0	
	$\overline{1}11$	$\overline{1}2\overline{1}3$	0.748	0.824	1.84	
$(11\overline{1})_{TiC}//(01\overline{1}0)_{M_7C_3}$	$11\overline{2}$	0001	0.529	0.454	0	9.8
	$\overline{1}10$	$\overline{1}2\overline{1}0$	0.611	0.688	0	
	$\overline{2}11$	$\overline{1}2\overline{1}3$	0.793	0.824	3.42	
$(111)_{TiC}//(0001)_{M_7C_3}$	$\overline{1}01$	$\overline{2}110$	0.611	0.688	0	11.2
	$\overline{1}10$	$\overline{1}2\overline{1}0$	0.611	0.688	0	
	$\overline{2}11$	$\overline{1}100$	10.58	11.92	0	
$(100)_{TiC}//(01\overline{1}0)_{M_7C_3}$	001	0001	0.432	0.454	0	23.1
	010	$\overline{1}2\overline{1}0$	0.432	0.688	0	
	011	$\overline{1}2\overline{1}3$	0.611	0.824	11.58	
$(100)_{TiC}//(0001)_{M_7C_3}$	011	$\overline{1}2\overline{1}0$	0.611	0.688	0	24.5
	$0\overline{1}1$	$\overline{1}010$	0.917	1.192	0	
	001	$\overline{2}110$	0.432	0.688	15	

Fig. 3 XRD spectrum of A$_3$ sample

with the increase of TiC particles. When the addition of TiC particles exceeds 1.0 wt.%, the change of microstructure is not obvious. Moreover, when TiC particles are added into the melt, it still exists in the conformation of TiC and does not form the new phase, as shown in Fig. 3. The refinement of M$_7$C$_3$-type carbides in HHCCIs lies mainly on the action of TiC particles.

The main reasons that TiC additions can refine the carbides of HHCCIs are as follows. After adding TiC particles in the melt, TiC does not decompose and can form the new phase. It still exists in the conformation of TiC. TiC belongs to the binary high-melting interstitial transition metal compound. Its structure is face-centered cubic (FCC) lattice with the lattice parameter $a = 0.46$ nm. The M$_7$C$_3$-type carbides have the close-packed hexagonal structure with the lattice parameter $a = 0.688$ nm and $c = 0.454$ nm. The value of the two-dimensional lattice misfit is used to estimate whether some inclusions can act as the heterogeneous nuclei (Ref 21, 22). A mathematical model of the two-dimensional lattice misfit is (Ref 23, 24):

$$\delta^{(hkl)_s}_{(hkl)_n} = \sum_{i=1}^{3} \frac{\left| d^i_{[uvw]_s} \cos \theta - d^i_{[uvw]_n} \right| / d^i_{[uvw]_n}}{3} \times 100 \quad \text{(Eq 2)}$$

where $(hkl)_s$ is the low index crystal face of the nucleus, $[uvw]_s$ is the low index crystal orientation in the $(hkl)_s$, $(hkl)_n$

is the low index crystal face of the new crystal phase, the $[uvw]_n$ is the low index crystal orientation in the $(hkl)_n$, $d_{[uvw]_s}$ and $d_{[uvw]_n}$ are the atomic spacing along the $[uvw]_s$ and the $[uvw]_n$, respectively, θ is the angle included between the $[uvw]_s$ and the $[uvw]_n$ (θ < 90°).

Bramfitt (Ref 24) proposed a theory that the nuclei were most effective when the mismatch was less than 6%, less effective when the mismatch was between 6 and 12%, and useless above 12%. Table 1 shows the calculation of the lattice misfit δ between $(110)_{TiC}$ and $(01\overline{1}0)_{M_7C_3}$. It can be seen that the lattice misfit between $(110)_{TiC}$ and $(01\overline{1}0)_{M_7C_3}$ is 8.4% and the lattice misfit between $(11\overline{1})_{TiC}//(01\overline{1}0)_{M_7C_3}$ is 9.8%. Therefore, TiC can act as heterogeneous nuclei of the primary M$_7$C$_3$ carbide and refine primary carbides. Furthermore, many reports show TiC can act as the substrate for the heterogeneous nucleation of MC carbide and M$_3$C carbide in white cast iron and steel (Ref 25-27) and even has some crystallographic relationship with austenite in high Cr WCIs (Ref 28). It has been well recognized that the M$_7$C$_3$ carbide in the hypereutectic high chromium cast iron is hexagonal lattice and oriented with the zone axis [0001]; therefore, the M$_7$C$_3$ carbide will grow to be long rod shape (Ref 1, 10, 25). For this reason, it can be deduced that the TiC particles may also be attached to the primary carbides in some other place of the long rod. Figure 4 is the schematic illustration of lattice correspondence of TiC and M$_7$C$_3$. Figure 5 shows TiC and M$_7$C$_3$-type carbide combine compactly together. Figures 6 and 7 are diffraction spots of the two phases, respectively. By calculation and calibration, above two phases are TiC and M$_7$C$_3$-type carbide, respectively. M$_7$C$_3$-type carbide is the hexagonal lattice structure and its reciprocal vector is [0001]. TiC is the face-centered cubic structure and its reciprocal vector is [001]. In the interface of two phases in Fig. 5, the selected diffractions of the two phases zone are shown in Fig. 8. The diffraction spots in Fig. 8 consist of two sets of different spots. In fact, the diffraction spots in Fig. 8 are the supraposition of Fig. 6 and 7.

Moreover, the diameter of added TiC particles in the melt is about 2.8 μm, and the dimension of TiC particles in the hypereutectic high chromium cast irons is obviously smaller than 2.8 μm, as shown in Fig. 5. The main reason is that the TiC particles produce local solution when they are added into
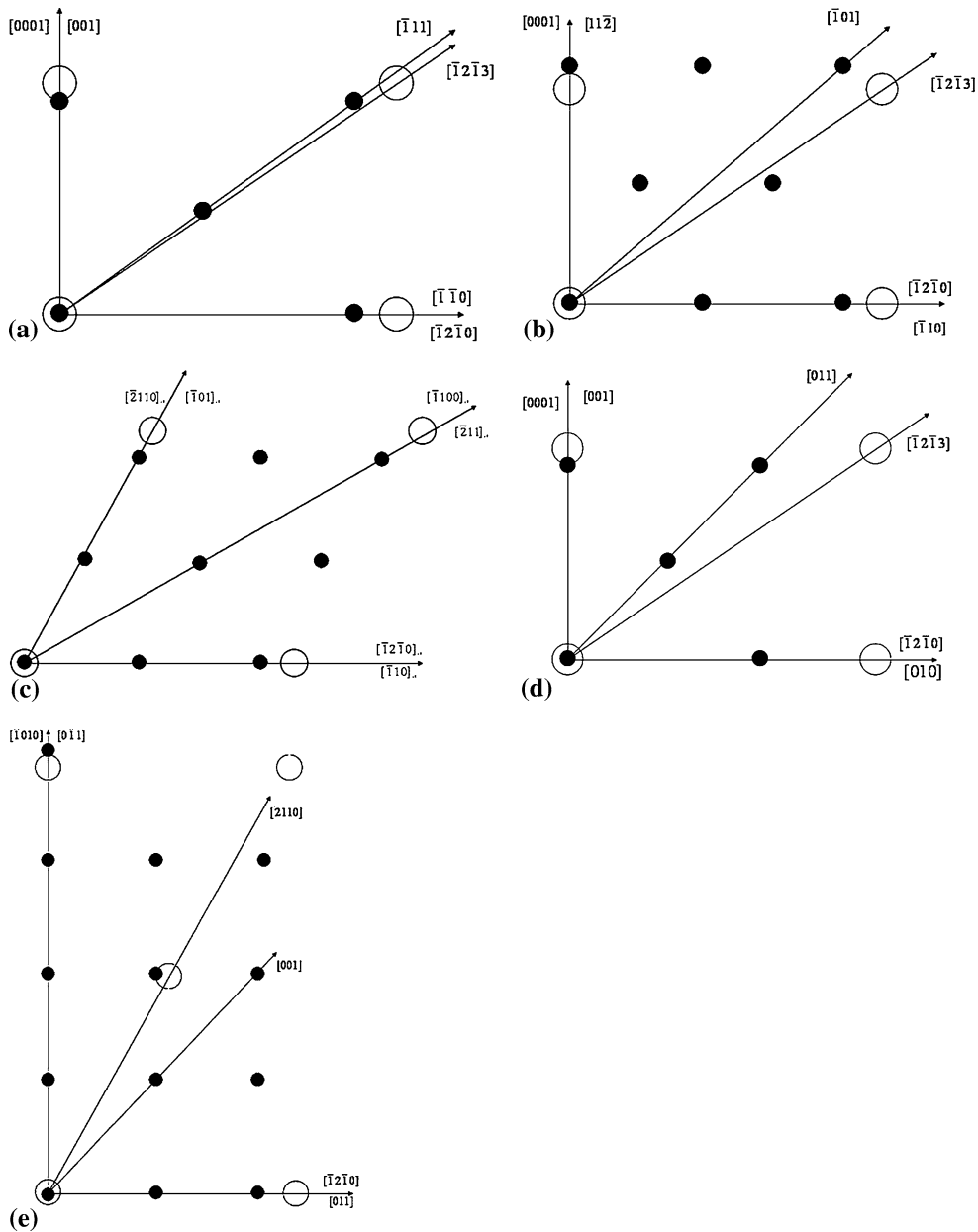
Fig. 4 Schematic illustration of lattice correspondence of TiC and M_7C_3: (a) $(110)_{TiC}//(01\bar{1}0)_{M_7C_3}$; (b) $(11\bar{1})_{TiC}//(01\bar{1}0)_{M_7C_3}$; (c) $(111)_{TiC}$ and $(0001)_{M_7C_3}$; (d) $(100)_{TiC}$ and $(01\bar{1}0)_{M_7C_3}$; (e) $(100)_{TiC}$ and $(0001)_{M_7C_3}$ (○: representing the tetrahedron or octahedron of M_7C_3; ●: representing the Ti atom in the TiC) (Ref 25)

the melt. The solution of TiC particles only happens at the surface contacting with the melt. Because the holding time of melt is short (only 5 min), the TiC particles do not dissolve completely and only their dimensions were diminished.

3.2 Effect of TiC Additions on Mechanical Properties of HHCCIs

Figures 9 and 10 show the effect of TiC additions on the hardness and impact toughness of HHCCIs. The hardness of HHCCIs shows a slight increase and impact toughness shows an obvious increase with the increase of TiC additions. However, when the addition of TiC particles exceeds 1.0 wt.%, the impact toughness of HHCCIs shows no obvious change.

The hardness of high Cr WCIs depends on the hardness of matrix and carbide volume fraction (Ref 29). The matrix of HHCCIs consists of the martensite and austenite. The addition of TiC particles has no obvious effect of the structure of matrix, which still consists of the martensite and austenite. Moreover, the solution of TiC particles has no obvious effect on the microhardness of matrix, as shown in Fig. 11. The main reason is the solution amount of TiC particles is very small while contacting with HHCCIs melt because of short holding time of melt. The volume fraction of carbide in the HHCCIs shows a slight increase with the addition of TiC particles, as shown in Fig. 12. However, the matrix shows no obvious change and its microhardness shows no obvious increase even when the TiC particles are added into the melt. So, the macrohardness of
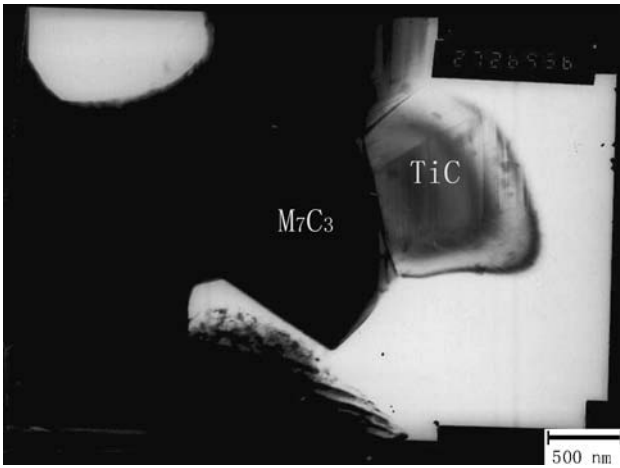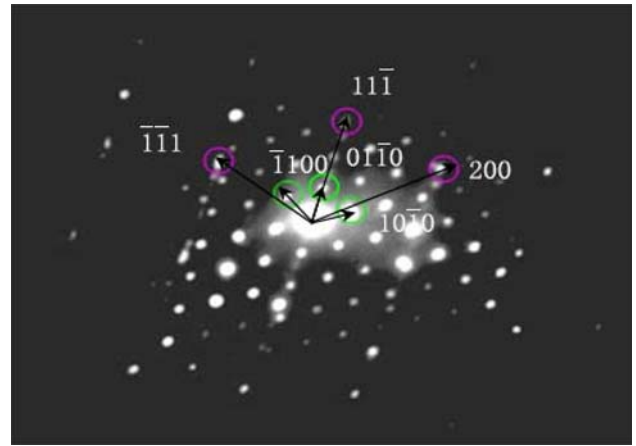
Fig. 5 The TEM of A$_3$ sample
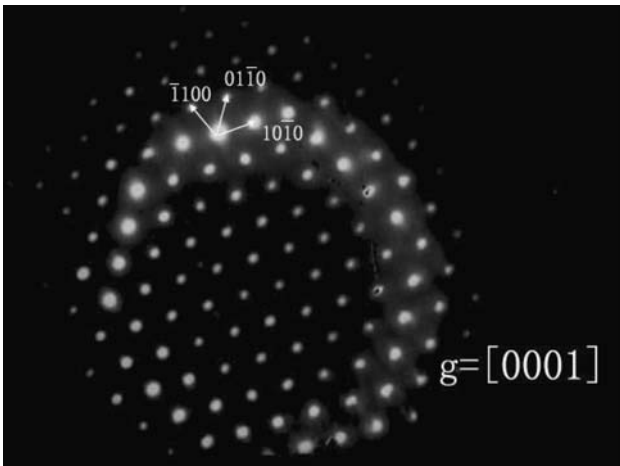
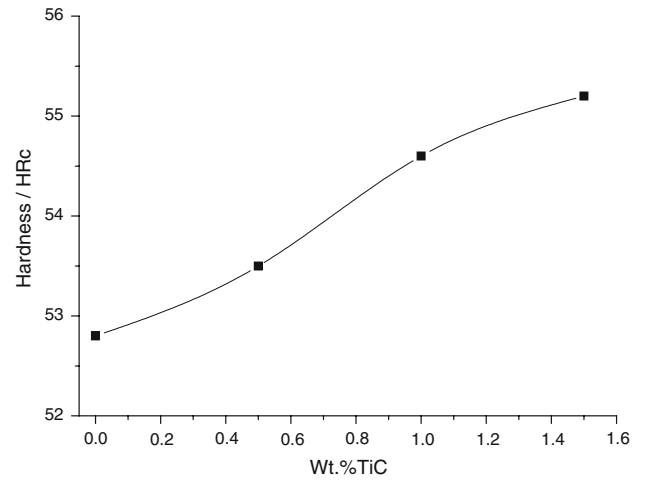**Fig. 6** Diffraction spot of M$_7$C$_3$-type carbide
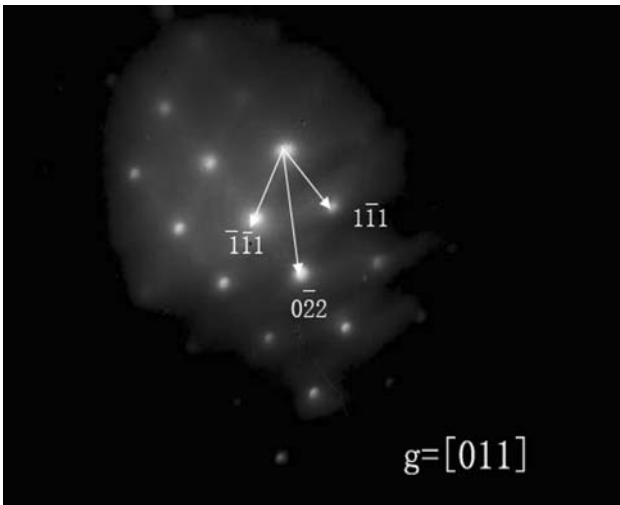
Fig. 7 Diffraction spot of TiC

HHCCIs shows only a slight increase with the addition of TiC particles.
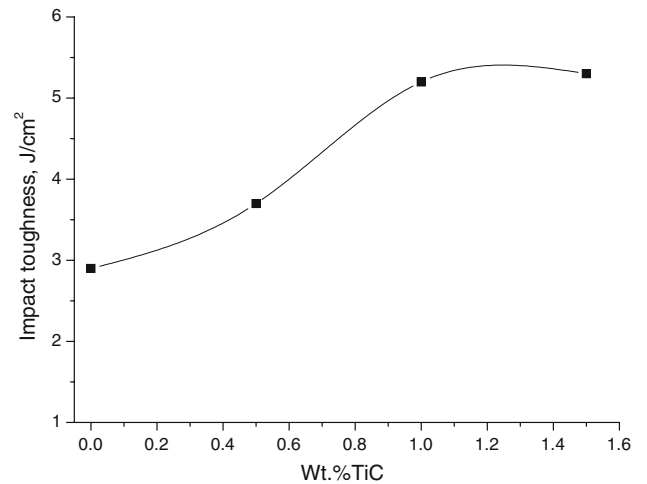
The reason for the above-mentioned impact test results can be explained as follows: The theory of fracture mechanics

**Fig. 8** The selected diffractions of the two phases zone

**Fig. 9** Effect of TiC additions on as-cast hardness

Fig. 10 Effect of TiC additions on impact toughness of HHCCIs samples tempering at 200 °C for 4 h

points out that brittle fracture includes the initiation and propagation of crack (Ref 30, 31), which is determined by matrix and the amount, morphology, and size of carbides in
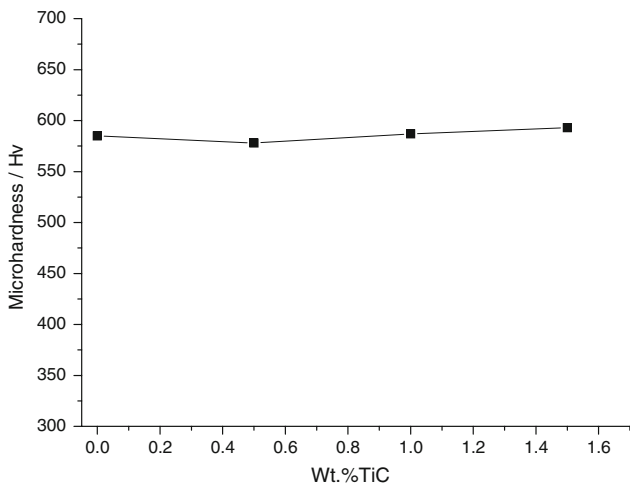
Fig. 11 Effect of TiC additions on microhardness of matrix of as-cast HHCCIs
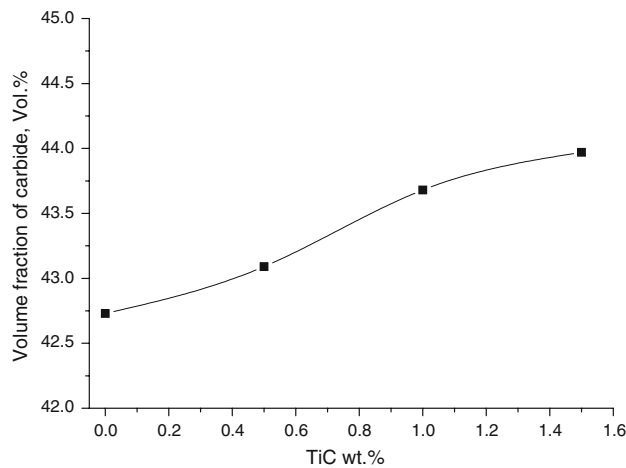
Fig. 12 Effect of TiC addition on volume fraction of carbide in the HHCCIs

white cast iron (Ref 32). In the ordinary HHCCIs with no addition of TiC particles, the carbide is coarse. The crack can easily propagate along the carbides and the toughness is relatively low. The carbide is gradually refined with the addition of TiC grains. The crack is difficult to propagate, the toughness improves correspondingly. When the addition of TiC grains exceeds 1.0%, the refinement of carbide is slight and the volume fraction of carbide in the HHCCIs has a slight increase, the former can lighten the propagation of crack and increase the impact toughness, but the latter can accelerate the propagation of crack and decrease the impact toughness. The comprehensive action of above two aspects results in that the impact toughness of HHCCIs has no obvious change when the addition of TiC particles exceeds 1.0%.

4. Conclusions

(1) The carbides in the HHCCIs are refined gradually and the shape of the primary M_7C_3-type carbides became more isotropic with the increase of TiC particles. When the addition of TiC particles exceeds 1.0 wt.%, the change of carbides is not obvious.

(2) The macrohardness of HHCCIs shows a slight increase, the microhardness of matrix shows no obvious change and impact toughness shows an obvious increase with the increase of TiC additions. When the addition of TiC particles exceeds 1.0 wt.%, the impact toughness shows no obvious change.

Acknowledgments

References

1. O.N. Dogan, J.A. Hawk, and G. Laird II, Solidification Structure and Abrasion Resistance of High Chromium White Irons, *Metall. Mater. Trans. A*, 1997, **28A**(6), p 1315–1328
2. R.J. Llewellyn, S.K. Yick, and K.F. Dolman, Scouring Erosion Resistance of Metallic Materials in Slurry Pump Service, *Wear*, 2004, **256**(6), p 592–599
3. A. Royer, J.M. Schissler, P. Camelin, S. Vasseur, and J. Saverna, Relations Between Microstructure and Wear Resistance of White Cast-Irons (28%Cr) for the Low-Speed Transport of Abrasive Materials, *Wear of Materials: International Conference on Wear of Materials*, 1985, p 634–644
4. A.S.H. Mousavi, A. Bahrami, N. Varahram, and P. Davami, Effects of Tungsten on Erosion-Corrosion Behavior of High Chromium White Cast Iron, *Mater. Sci. Eng. A*, 2007, **454–455**, p 623–628
5. J.K. Fulcher, T.H. Kosel, and N.F. Fiore, The Effect of Carbide Volume Fraction on the Low Stress Abrasion Resistance of High Cr-Mo White Cast Irons, *Wear*, 1983, **84**(3), p 313–325
6. J.D. Xing, W.H. Lu, and X.T. Wang, *Proceedings of the International Conference on Wear of Materials*, ASME, New York, 1983, p 45
7. N.I. Kitaigora, Impact-Abrasion Wear Resistance of High-Chromium Cast Iron, *Met. Sci. Heat Treat.*, 1975, **17**(5–6), p 417–420
8. X.H. Zhi, J.D. Xing, Y.M. Gao, and H. Zhou, *Low Cost, High-Wearability Hypereutectic High Chromium Cast Iron and Its Production Method*, CN1769508-A, 10 November 2005
9. S. Zhang, W. Huang, Z. Zhao, Y. Zhao, and H. Wang, Technology to Overcome the Brittleness of Super High Chromium White Cast Iron, *Foundry Technol.*, 2004, **25**(6), p 408–410
10. X.J. Wu, J.D. Xing, H.G. Fu, and X.H. Zhi, Effect of Titanium on the Morphology of Primary M_7C_3 Carbides in Hypereutectic High Chromium White Iron, *Mater. Sci. Eng. A*, 2007, **457**(1–2), p 180–185
11. X.H. Zhi, J.D. Xing, H.G. Fu, and B. Xiao, Effect of Niobium on the As-Cast Microstructure of Hypereutectic High Chromium Cast Iron, *Mater. Lett.*, 2008, **62**(5–6), p 857–860
12. Y.H. Qu, J.D. Xing, X.H. Zhi, J.Y. Peng, and H.G. Fu, Effect of Cerium on the As-Cast Microstructure of a Hypereutectic High Chromium Cast Iron, *Mater. Lett.*, 2008, **62**, p 3024–3027
13. S. Atamert and H.K.D.H. Bhadeshia, Silicon Modification of Iron Base Hardfacing Alloys, in *Recent Trends in Welding Science and Technology (TWR'89)*, A. David and J.M. Vitek, Eds., Materials Park, Ohio, 1990, p 273–278
14. S. Atamert, and H.K.D.H. Bhadeshia, Wear Resistance and Microstructure of Fe-Cr-C and Fe-Cr-Si-C Hardfacing Alloys, *Proceedings of Heat Treatment*, The Institute of Metals, London, 1987, p. 39–43
15. Y. Ma, F. Zhao, J. Pan, Y. Liu, J. Li, and Z. Li, Study on Carbides Growth Mechanism and Influencing Factors of Hypereutectic High Chromium White Cast Irons, *Hot Work. Process*, 2007, **36**(1), p 14–16
16. H. Fusheng and W. Chaochang, Modifying High Cr-Mn Cast Iron with Boron and Rare Earth-Si Alloy, *Mater. Sci. Technol.*, 1989, **5**(9), p 918–924
17. Y. Li, Q. Jiang, Y. Zhao, Z. He, and X. Zhong, Influence of Boron on Solidification Structures of M2 High Speed Steel, *Chinese J. Mater. Res.*, 1999, **13**(2), p 183–187

18. J. Zhang, D. Li, J. Zhao, J. Jia, and J. Li, Structural Feature of As-Cast High Cr Injection Microalloy Martensitic Cast Iron, *Acta Metall. Sin.*, 1990, **26**(6), p B406–B410

19. S. Xu, S. Jiang, M. Liu, and L. Huang, A Primary Study of the Spray Suspension Method to Cast Low Chromium Cast Iron-Matrix Tungsten Carbide Particle-Reinforced Composites, *J. Dalian Railway Inst.*, 1987, (2), p 7–12

20. M. Yang, F. Pan, L. Bai, and H. Yang, Effects of TiC Particles on As-Cast Microstructure, Mechanical Properties and Solidification Behavior of ZA84 Magnesium Alloy, *Spec. Cast. Nonferrous Alloys*, 2007, **27**(11), p 821–823

21. Q. Yang, B. Liao, J. Liu, and M. Yao, Effect of Rare Earth Elements on Carbide Morphology and Phase Transformation Dynamics of High Ni-Cr Alloy Cast Iron, *J. Rare Earths*, 1998, **16**(1), p 36–40

22. Q. Yang, B. Liao, Z. Cui, M. Yao, and X. Wan, Effect of Freezing Point on RE Inclusion as Heterogeneous Nucleation of Primary Austenite in Fe-C Alloys, *Chinese J. Mater. Res.*, 1999, **13**(4), p 353–358

23. D. Turnbull and B. Vonnegut, Nucleation Catalysis, *Ind. Eng. Chem.*, 1952, **44**(6), p 1292–1298

24. B.L. Bramfitt, Planar Lattice Disregistry Theory and Its Application on Heterogistry Nuclei of Metal, *Metall. Trans*, 1970, **1**(7), p 1987–1995

25. X.H. Zhi, *Study on the Morphology Control of Primary Carbides in Hypereutectic High Chromium Cast Irons*, Xi'an Jiaotong University, Xi'an, 2008

26. Z. Xu, G. Liang, Q. Guan, and Q. Jiang, TiC as Heterogeneous Nuclei of the (Fe, Mn)$_3$C and Austenite Intergrowth Eutectic in Austenite Steel Matrix Wear Resistant Composite, *Mater. Res. Bull.*, 2004, **39**, p 457–463

27. Y. Li, Q. Jiang, Y. Zhao, and Z. He, Influence of Ti on MC carbide in M2 steel, *J. Mater. Sci. Technol.*, 1997, **13**(6), p 471–474

28. S. Huang, Research on High Chromium Cast Iron Inoculated with Vanadium-Titanium-Boron, *Mod. Cast Iron*, 2001, (4), p 19–21

29. S.J. Hao, *High Chromium Abrasive Wear Resistant Cast Irons*, Coal Industry Press, Beijing, 1993

30. P.D. Zavattieri and H.D. Espinosa, Grain Level Analysis of Crack Initiation and Propagation in Brittle Materials, *Acta Mater.*, 2001, **9**(20), p 4291–4311

31. H. Qiu, H. Mori, M. Enoki, and T. Kishi, Fracture Mechanism and Toughness of the Welding Heat-Affected Zone in Structural Steel Under Static and Dynamic Loading, *Metall. Mater. Trans. A*, 2000, **1A**(11), p 2785–2791

32. R.H. Frost and G.K. Tmajewski, Impact Fracture Behavior of High Chromium-Molybdenum White Cast Iron, *AFS Trans.*, 1986, **94**, p 292–297